

Supplementary Material for “Flux states and topological phases from spontaneous time-reversal symmetry breaking in CrSi(Ge)Te₃-based systems”

I. PROJECTED DENSITY OF STATES, ORBITAL CHARACTER ANALYSIS AND BAND-INVERSIONS

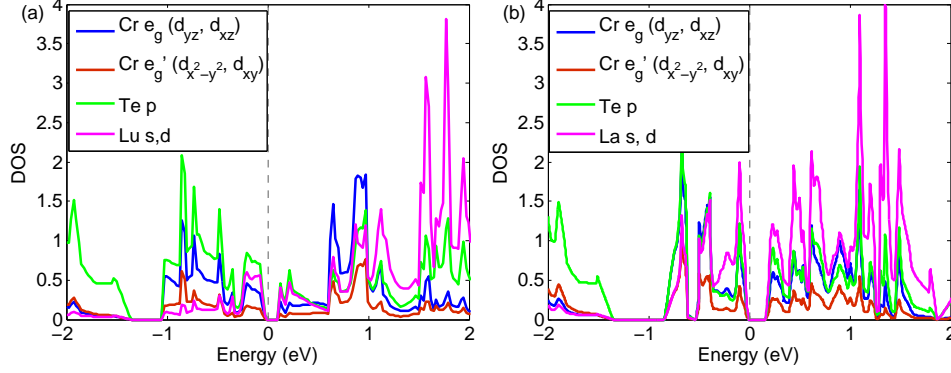


FIG. 1: Local density of states projected onto various orbitals in the majority-spin channel, (a) for 1 ML Lu deposited on single-layer CrGeTe₃, and (b) for 1 ML La deposited on single-layer CrSiTe₃. The Fermi level is at $E = 0$.

In this section, we make a detailed analysis of the orbital character as well as band-inversion character of 1 mono-layer (ML) La deposited on single-layer (SL) CrSiTe₃ and 1 ML Lu deposited on SL CrGeTe₃. Following the convention introduced in the main text, we call these two systems “Si-La” and “Ge-Lu” for simplicity. We first review the electronic structure of bulk CrSiTe₃ (CrGeTe₃). In the ionic crystal picture, the on-site Coulomb repulsion between the Cr 3d electrons (~ 3.5 eV) pushes the 3d orbitals in the minority spin channel far above the Fermi level. The important physics of the system is thus dominated by the 3d orbitals in the majority spin channel. The five-fold degenerate majority-spin 3d orbitals are then split into a_{1g} (d_{z^2}), e_g (d_{yz} and d_{xz}) and e'_g ($d_{x^2-y^2}$ and d_{xy}) levels in the rhombohedral crystal field environment. The magnetic moment of CrSiTe₃ (CrGeTe₃) was reported to be ~ 2.73 (2.80) μ_B per Cr atom, [1, 2] suggesting that Cr is a 3+ cation in these compounds. The remaining three electrons on the Cr ion then occupy the majority-spin a_{1g} and e'_g orbitals, giving rise to $\sim 3 \mu_B$ for each ion. We assume a 2- oxidation state for Te, with the Te p orbitals fully occupied and lying somewhat below the Fermi level. The four empty e_g states (from the two Cr sites) in the majority spin channel are located immediately above the Fermi level, leading to an indirect gap ~ 0.4 eV for CrSiTe₃ as reported in Ref. 3.

If 1 ML La (Lu) is deposited on SL CrSiTe₃ (CrGeTe₃), the La (Lu) atom tends to donate two of its three valence electrons to the unoccupied Cr e_g (d_{yz} and d_{xz}) orbitals, making the four majority-spin e_g states half filled, while the remaining electron occupies the 5d or 6s orbitals of the adatom also in the majority-spin channel. Therefore, with adatoms deposited, there are five physically important states around the Fermi level, namely, the two occupied Cr e_g states, the one occupied s or d state from the adatom, and the two unoccupied Cr e_g states, all in the majority spin channel.

However, as discussed in the main text, CrSiTe₃ and CrGeTe₃ have a strongly covalent character, as the hybridization between Cr 3d and Te 4p orbitals is fairly strong. The above analysis based on the ionic crystal picture can be carried over, except that the states around the Fermi level no longer have simple orbital character. In Fig. 1 we show the local density of states (DOS) for the Ge-Lu (Fig. 1(a)) and Si-La (Fig. 1(b)) systems projected onto various atomic orbitals in the majority-spin channel. The states around the Fermi level have significant contributions from both Cr d and Te p orbitals, and the Lu (La) s and d orbitals also play important roles. It follows that the hybridization effects in these two systems are strong, so the influence of nonlocal Coulomb interactions is expected to be significant.

Figs. 2(a) and (b) show the spin-majority bandstructures for the Ge-Lu and Si-La systems projected

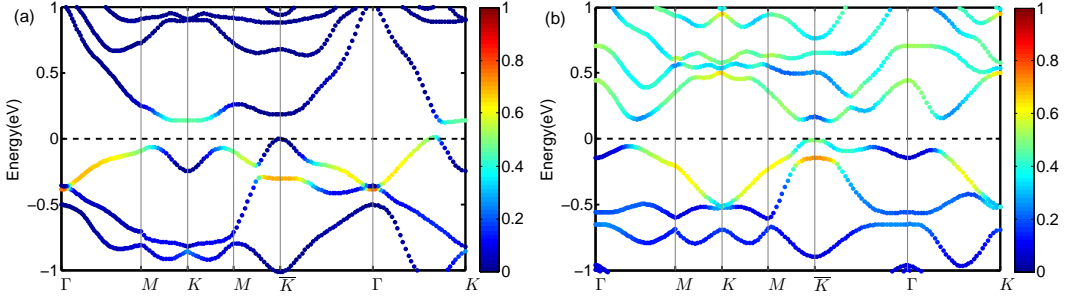


FIG. 2: Majority-spin bandstructures of (a) Ge-Lu projected onto Lu s orbitals, and (b) Si-La projected onto La d orbitals.

onto Lu s and La d orbitals respectively. Clearly there is a band-inversion character at Γ for Si-La and at K for Ge-Lu.

II. HYBRID FUNCTIONALS, WANNIERIZED TIGHT-BINDING MODELS, SURFACE STATES, ANOMALOUS HALL CONDUCTIVITY, AND INTER-SITE CURRENTS

The main results in the letter are obtained using a hybrid-functional extension of density-functional theory (DFT). In the hybrid-functional approach, the exchange part of the screened Coulomb interaction is treated as a weighted average in which a fraction is treated using nonlocal Hartree-Fock exchange and the remainder is calculated from a conventional semilocal-density functional. The hybrid-functional approach has been shown to be more successful than traditional DFT in predicting various physical properties such as energy gaps, lattice parameters and magnetic moments [4, 5]. In our calculations, a $6 \times 6 \times 1$ \mathbf{k} mesh and a 380 eV energy cutoff are adopted, and a slab geometry is used for all the systems.

We then use the Wannier90 code package [6, 7] to generate realistic tight-binding (TB) models for the Si-La and Ge-Lu systems. These TB models are “realistic” in the sense that the bandstructures from the TB models exactly reproduce those from first-principles calculations within an energy window that extends from -1.5 eV below to $+1.5$ eV above the Fermi level. The Bloch functions obtained from the first-principles calculations are projected onto Cr s , Cr d , Te p , Si (Ge) p , and La (Lu) s and d orbitals to construct the corresponding Wannier functions in each spin channel. Then one can extract the hopping parameters of the 42-band TB model in each spin channel for each system, and calculate various physical quantities using such TB models.

In order to calculate the edge states as shown in Fig. 5(a) and (c) in the main text, we truncate the Wannierized TB models in the (010) direction, and the semi-infinite spectral functions are calculated using the iterative Green’s-function method reported in Ref. 8. The anomalous Hall conductivities shown in Fig. 5(b) and (d) of the main text are calculated using the Wannier-interpolation method proposed by Wang *et al.*[9]

The inter-site current is also calculated in the Wannier basis. The net current flowing onto site j can be expressed as

$$\begin{aligned}
 \frac{dn_j}{dt} &= \text{Tr} \left[\frac{d\hat{n}_j}{dt} \hat{\rho} \right] \\
 &= \sum_{j',m} \langle W_{mj'} | \frac{i}{\hbar} [H, \hat{n}_j] \hat{\rho} | W_{mj'} \rangle \\
 &= \frac{i}{\hbar} \sum_m \langle W_{mj} | [\hat{\rho}, H] | W_{mj} \rangle \\
 &= \frac{i}{\hbar} \sum_{j'} \sum_{m,m'} (\rho_{mj,m'j'} H_{m'j',mj} - H_{mj,m'j'} \rho_{m'j',mj}) \\
 &= \sum_{j'} F_{j'j}, \tag{1}
 \end{aligned}$$

TABLE I: Orbital occupations in the GGA ground state for the Ge-Lu system

	d_{xz}	d_{yz}	p_x	p_y	p_z
Cr1 (0,0)	0.857	0.857	-	-	-
Cr2 (0.333, 0.667)	0.812	0.812	-	-	-
bottom Te1 (0.667, -0.033)	-	-	0.708	0.620	0.873
bottom Te2 (0.033, 0.700)	-	-	0.700	0.627	0.874
bottom Te3 (0.300, 0.333)	-	-	0.583	0.745	0.874
top Te1 (0.322, -0.038)	-	-	0.772	0.678	0.813
top Te2 (0.640, 0.678)	-	-	0.751	0.699	0.813
top Te3 (0.038, 0.360)	-	-	0.651	0.798	0.813

where j and j' run over atomic sites and m is the index of Wannier functions on each site, with $|W_{mj}\rangle$ representing the m th Wannier function located at site j . H is the Hamiltonian, and $\hat{n}_j = \sum_m |W_{mj}\rangle\langle W_{mj}|$ is the number operator on site j . $\hat{\rho}$ is the density operator; at zero temperature, $\hat{\rho}$ can be expressed in terms of the occupied Bloch states as $\hat{\rho} = A_0 \int d^2k/(2\pi^2) \sum_n |\psi_{n\mathbf{k}}\rangle\langle\psi_{n\mathbf{k}}| \theta(\epsilon_f - \epsilon_{n\mathbf{k}})$, where $|\psi_{n\mathbf{k}}\rangle$ and $\epsilon_{n\mathbf{k}}$ are the Bloch state and the corresponding band energy, ϵ_f is the Fermi level ($\theta(x) = 1$ for $x > 0$, and $\theta(x) = 0$ otherwise), and A_0 is the area of the primitive cell. $\rho_{mj,m'j'}$ and $H_{mj,m'j'}$ are the matrix elements of the density operator and the Hamiltonian in the Wannier basis. In the last line of Eq. (1), $F_{j'j} = (-2/\hbar) \sum_{m,m'} \text{Im}[\rho_{mj,m'j'} H_{m'j',mj}]$ is interpreted as the current flowing between site j and j' . It should be noted that the Wannier functions are constructed by directly projecting the Bloch bands within some energy window onto the chosen atomic orbitals without the maximal localization procedure. Thus the Wannier functions can be considered as atomic orbitals centered at the lattice sites, and it is legitimate to interpret the current flows $F_{j'j}$ in the Wannier basis as the inter-site current.

III. ELECTRONIC STRUCTURES WITH SEMI-LOCAL EXCHANGE-CORRELATION FUNCTIONALS AND ORBITAL ORDERING

In this section, we present the bandstructures of the Si-La and Ge-Lu systems calculated by traditional semilocal exchange-correlation functionals. To be specific, we have calculated the bandstructures for both systems using three different type of semilocal exchange-correlation functionals. We first adopt the PerdewBurkeErnzerhof-type of generalized gradient approximation (GGA) [10] to treat the exchange and correlations. Then we use the rotationally invariant implementation of the ‘‘DFT+ U ’’ [11] method for a better treatment on the Cr 3d orbitals. In the end, we apply the HSE[12] hybrid functionals with a short screening length of Coulomb interactions $\lambda = 1\text{\AA}$. Even though the HSE hybrid functional is essentially nonlocal, we still call it ‘‘semilocal’’ because a short screening length $\sim 1\text{\AA}$ is adopted so that the Coulomb interactions can be approximated as onsite.

The Wannierized bandstructures for both Si-La and Ge-Lu systems calculated using these three semilocal functionals are shown in Fig. 4 and Fig. 3 respectively. First of all, we notice that both systems are predicted to be metallic by all the three semilocal functionals. However, if one only looks at the spin-majority bands (blue lines), one may notice that the spin-majority bands are already gapped at the GGA level (Fig. 4(a) and Fig. 3(a)). Such gapped GGA ground states in the majority spin channel are associated with the breaking of C_3 symmetry and some ‘‘orbital ordering’’ of Te p orbitals.

In order to understand the pattern of the orbital order in the GGA ground states, we have calculated the orbital occupation number in the majority spin channel $\langle \hat{n}_{l\uparrow} \rangle$ in the Wannier-function basis, where $\hat{n}_{l\uparrow}$ is the number operator of the l th Wannier function of majority spin [17]. As discussed in Sec. I, the La or Lu adatom tends to donate two of the three valence electrons to the monolayer system so that the four majority-spin Cr e_g orbitals in the conduction band become half filled (if the system were considered as ionic crystals). Thus one may expect that the system would become orbital ordered through the kinetic exchange mechanism [13] with alternating d_{xz} and d_{yz} orbitals on the two Cr sublattices, and possibly with weak Jahn-Teller distortions in the Te octahera. However, our calculations indicate that the d_{xz} and d_{yz} orbitals are equally occupied on both Cr sites; instead the orbital ordering shows up in the Te layers. To be specific, the electrons at two of the three bottom/top Te atoms have more p_x character, while it has a stronger p_y character at the third bottom Te atom.

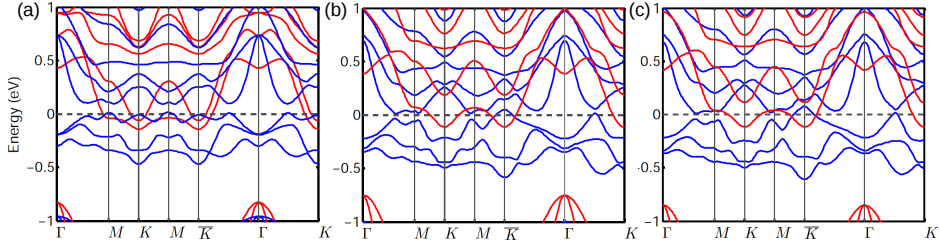


FIG. 3: Bandstructures of the Ge-Lu system in the absence of spin-orbit coupling with different exchange-correlation functionals: (a) GGA, (b) GGA+ U , and (c) HSE hybrid functional with the screening length $\lambda=1\text{\AA}$. The blue and red lines represent the spin-majority and spin-minority bands respectively.

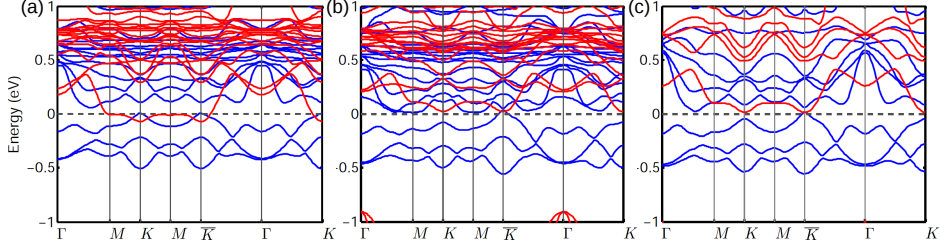


FIG. 4: Bandstructures of the Si-La system in the absence of spin-orbit coupling with different exchange-correlation functionals: (a) GGA, (b) GGA+ U , and (c) HSE hybrid functional with the screening length $\lambda=1\text{\AA}$. The blue and red lines represent the spin-majority and spin-minority bands respectively.

The orbital occupations for all the Cr e_g and Te p orbitals in the majority spin channel are shown in Table. I for the Ge-Lu system. The corresponding in-plane atomic positions in reduced coordinates are also given in the table. Clearly the e_g orbitals (d_{xz} and d_{yz}) are equally occupied for both Cr sites, while Te p_x and p_y orbitals show ordering pattern in both top and bottom atomic layers. In the top layer, the Te atom at (0.038, 0.360) has a stronger p_y character, while the other two have more p_x occupations; in the bottom layer, the Te atom at (0.300, 0.333) is “ p_y -like”, while the other two are “ p_x -like”. The spontaneous C_3 symmetry breaking remains robust in GGA+ U and hybrid-functional (with both short and long screening lengths) treatments. We believe such novel orbital ordering in the Te layers are unique features of such transition-metal tellurides with strong $p-d$ hybridizations and covalent character. It worth to note that such orbital-ordered ground state is not unique: applying a C_3 operation would lead to an equivalent ground state, so that there is three-fold degeneracy in the ground state.

Applying local Coulomb interactions [14] to the Cr $3d$ orbitals does not make significant changes to the GGA bandstructures. At the first glance the GGA+ U bands of the majority spin become metallic (Fig. 3(b) and Fig. 4(b)), otherwise they look similar to those from GGA. This is not surprising because the dominant interaction among $3d$ electrons is the Hubbard U , which is exerted on electrons of the same orbital character with opposite spins. The occupied states around the Fermi level are spin polarized implying that Hubbard U would play a minor role. On the other hand, while orbital time-reversal symmetry is preserved in the GGA ground states in the majority spin channel, it is already broken in the GGA+ U states as shown in Fig. 3(b) and Fig. 4(b) (the energies of the majority spin at \mathbf{k} and $-\mathbf{k}$ are different). We argue that such spontaneous time-reversal symmetry breaking in the majority spin channel is due to the local Hunds’ rule interaction, the strength of which is $U' - J$ (U' is the inter-orbital repulsion, J is the local exchange interaction in the same spin species). If one does Hartree-Fock treatment to Hunds’ rule interaction, the Fock term has the chance to pick up a complex value, thus may lead to a time-reversal-breaking ground state. The mechanism of time-reversal symmetry breaking is similar as that in (111) $\text{LaNiO}_3/\text{LaAlO}_3$ heterostructures as discussed in Ref. 15, although in their case the e_g orbitals are ($d_{x^2-y^2}$, d_{z^2}). As a consequence of the orbital time-reversal symmetry breaking, there are small antiferromagnetically ordered orbital moments on the Cr sites even in the absence of spin-orbit coupling. It is also interesting to note the GGA+ U bandstructures around the Fermi level are surprisingly similar to the hybrid-functional bandstructures with screening length $\lambda=1\text{\AA}$.

IV. ENERGY BANDS, ANOMALOUS HALL CONDUCTIVITIES, AND ORBITAL MOMENTS INCLUDING SPIN-ORBIT COUPLING

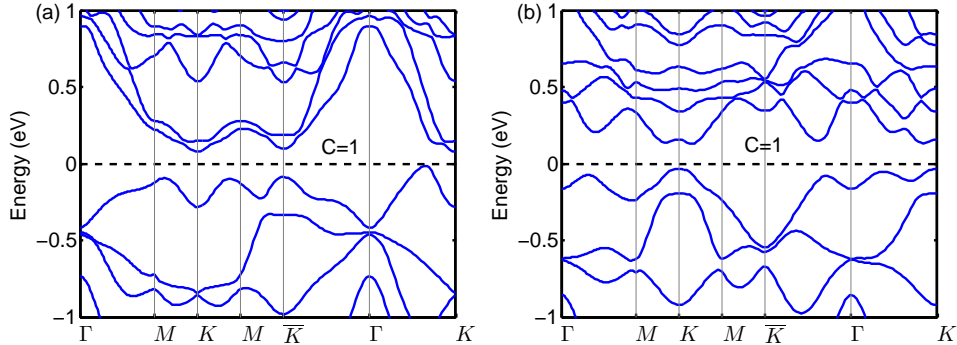


FIG. 5: Bandstructures when spin-orbit coupling is included, (a) for Ge-Lu, and (b) for Si-La. The Fermi levels are at $E = 0$.

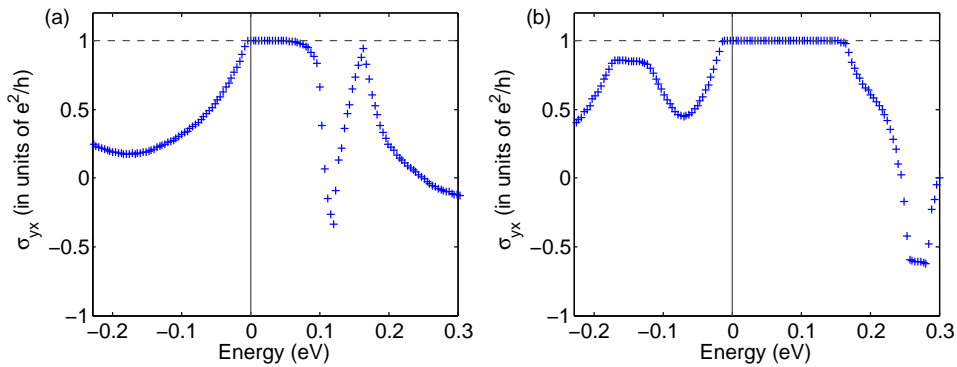


FIG. 6: The anomalous Hall conductivities including spin-orbit coupling for (a) Ge-Lu system, and (b) Si-La.

The spin-orbit-coupled bandstructures of Ge-Lu and Si-La are shown in Fig. 5(a) and (b) respectively. With spin-orbit coupling (SOC) included, the indirect gap for Ge-Lu decreases from ~ 70 meV to ~ 60 meV, while it increases from ~ 130 meV to ~ 160 meV for the Si-La system. The Chern numbers for both systems are $+1$. The anomalous Hall conductivities (σ_{yx}) for the Ge-Lu and Si-La systems are shown in Fig. 6(a) and Fig. 6(b) respectively. Clearly σ_{yx} in the gap is quantized at e^2/h for both systems. One may also notice that there is an abrupt sign change of σ_{yx} for the Ge-Lu system when the the Fermi level is placed in the conduction band. This results from the SOC-induced avoided crossings at ~ 0.1 eV around K and ~ 0.15 eV around \bar{K} as shown in Fig. 5(a). Such avoided crossings would lead to peaks of Berry curvature with opposite signs around K and \bar{K} , which are not at the same energy due to broken TR symmetry. This gives rise to the abrupt sign change of σ_{yx} shown in Fig. 6(a).

If we assume that the directions of the spin moments are not reversed after including SOC, then the choice of the Chern number becomes unique due to SOC. In other words, one of the two otherwise time-reversal-equivalent ground states with opposite Chern numbers becomes lower in energy. To be specific, we list the z components of the spin and orbital moments (denoted by M_S and M_L respectively) of different atomic sites for the two systems in the following two tables.

The spin and orbital moments for the Ge-Lu system are shown in Table II. When SOC is turned off, the ground state is a flux state with orbital moments $\{-0.126 \mu_B, 0.113 \mu_B\}$ for the two Cr sites, where the first moment refers to that of the adatom-covered Cr site. This is equivalent to the state with all the orbital moments flipped. When SOC is turned on, the two degenerate ground states become nondegenerate, and the orbital moments on the two Cr sites become $\{-0.120 \mu_B, 0.115 \mu_B\}$. Moreover, SOC tends to induce weak orbital moments on the three bottom Te sites, which sum to $0.018 \mu_B$, and are parallel to the corresponding on-site spin moments (which sum to $0.291 \mu_B$). As

TABLE II: Spin and orbital moments for the Ge-Lu system, in μ_B .

		Cr1	Cr2	Ge dimer	bottom Te	top Te	Lu
Without SOC	M_S	-3.767	-3.755	-0.094	0.282	0.041	-0.253
	M_L	-0.126	0.113	0.001	0.004	-0.003	-0.016
With SOC	M_S	-3.771	-3.762	-0.093	0.291	0.044	-0.249
	M_L	-0.120	0.115	0.001	0.018	0.003	0.000

TABLE III: Spin and orbital moments for the Si-La system, in μ_B .

		Cr1	Cr2	Ge dimer	bottom Te	top Te	La
Without SOC	M_S	-3.804	-3.729	-0.084	0.374	0.178	-0.636
	M_L	-0.066	0.082	0.000	0.001	-0.003	-0.180
With SOC	M_S	-3.805	-3.728	-0.081	0.369	0.177	-0.644
	M_L	0.071	-0.080	0.000	0.015	0.006	0.294

the p shell of a Te atom is more than half-filled, the orbital and spin moments tend to be parallel to maximize the energy gain from SOC according to Hund’s third rule.

The spin and orbital moments for the Si-La system are listed in Table III. Without SOC, the reported orbital moments on the two Cr sites are $\{-0.066 \mu_B, 0.082 \mu_B\}$, and the orbital moment on the La site is $-0.180 \mu_B$ and is associated with the La $5d$ electrons. Again, such a flux state is degenerate with its time-reversal (TR) partner with flipped orbital moments. When SOC is turned on, the signs of the orbital moments become reversed: the two Cr sites change from $\{-0.066 \mu_B, 0.082 \mu_B\}$ to $\{0.071 \mu_B, -0.080 \mu_B\}$, and the orbital moment on the La site changes from $-0.180 \mu_B$ to $0.294 \mu_B$. This results from the fact that the La $5d$ shell is less than half filled, so that the energy gain from SOC is maximized if the La on-site orbital moment ($0.294 \mu_B$) and spin moment ($-0.644 \mu_B$) are anti-parallel. Given that the SOC strength of La is much larger than that of Cr, the system evidently selects the state with anti-parallel spin and orbital moments on the La site.

V. FLUX STATES WITH TRIVIAL BAND TOPOLOGY

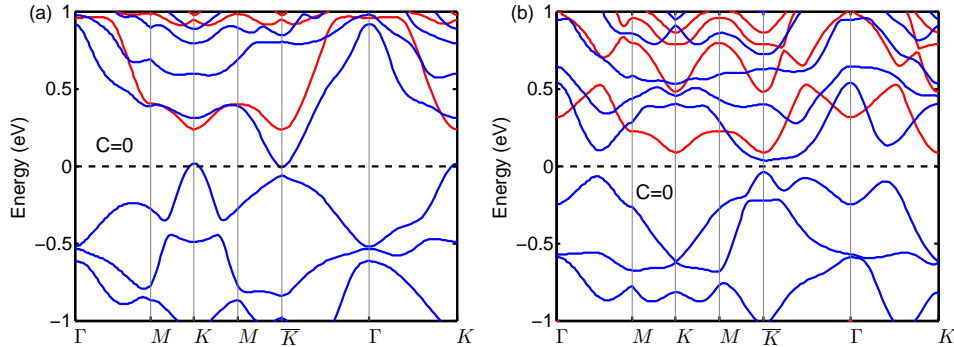


FIG. 7: Bandstructures for (a) 1 ML Lu deposited on single-layer CrSiTe_3 , and (b) 1 ML La deposited on single-layer CrGeTe_3 . The blue and red curves represent energy bands in the majority-spin and minority-spin channels.

As discussed in the main text, a flux state is not necessarily topologically nontrivial. For example, TR symmetry is broken in the majority-spin subspace in both 1 ML Lu deposited on SL CrSiTe_3 and 1 ML La deposited on SL CrGeTe_3 (denoted as “Si-Lu” and “Ge-La” for simplicity), and there are spontaneously generated current loops surrounding the Cr sites leading to antiferromagnetically ordered orbital moments. However, both of these systems are topologically trivial. Fig. 7(a) and (b) show the bandstructures in the absence of SOC for Si-Lu and Ge-La respectively. The blue (red) lines indicate the energy bands in the majority (minority) spin channel. It is straightforward to see that orbital TR symmetry is broken only in the majority spin channel, suggesting that the ground

states of the systems are flux states. However, orbital-character analysis (not shown) indicates that there is no band inversion in these systems, and that their computed Chern numbers remain zero.

VI. SCREENING-LENGTH DEPENDENCE OF THE STAGGERED ORBITAL MOMENTS AND TOPOLOGICAL INDICES

As discussed in the main text, the Coulomb interaction in the HSE hybrid functional is nonlocal, but is screened so as to have a finite range of the form $V(r) = (1 - \text{erf}(r/\lambda))/r$, where “erf” denotes the error function and λ is an effective screening length. In this section we present the details on the λ dependence of the orbital moments and Chern numbers. As shown in Fig. 8, the difference ΔM_{orb} between the orbital moments on the two Cr sublattices, which can be regarded as an order parameter for orbital antiferromagnetism, diminishes monotonically as the screening length is decreased. When $\lambda = 1 \text{ \AA}$, the orbital moments almost vanish, implying that inter-site currents for such short-range Coulomb interactions are negligibly small. Both systems remain topologically nontrivial down to $\lambda \sim 1.3 \text{ \AA}$, and eventually become trivial when $\lambda \leq 1 \text{ \AA}$.

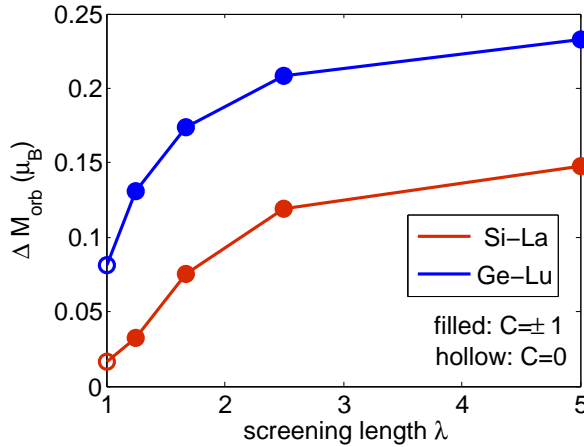


FIG. 8: The difference ΔM_{orb} between the orbital magnetic moments on the two Cr sites vs. the screening length λ (in \AA). Blue and red lines are for Ge-Lu and Si-La systems, and filled and hollow circles represent topologically nontrivial and trivial phases, respectively.

The corresponding bandstructures for the Si-La system without SOC at different screening lengths are shown in Fig. 9, where the blue and red lines represent the bands in the majority and minority spin channels respectively. As the screening length decreases, the gap at \bar{K} tends to decrease and becomes vanishing when $\lambda \approx 1.2 \text{ \AA}$ (see the inset in Fig. 9(c)). The gap then reopens as λ is further decreased indicating that the system is in a topologically trivial phase. Note that even though the system is metallic with slightly negative indirect gaps at $\lambda = 1.25 \text{ \AA}$ and $\lambda = 1 \text{ \AA}$, the Chern numbers are still well defined. One may also notice that the bandwidth around the Fermi level decreases with the screening length. This is because the nonlocal exchange interaction diminishes as the screening length decreases; then the “exchange-hole” effect [16] is suppressed, and effectively kinetic energy is reduced.

Similar bandstructures for the Ge-Lu system are shown in Fig. 10. The system already becomes metallic at $\lambda = 2.5 \text{ \AA}$ with negative indirect gap, but the Chern number of the spin-majority bands (blue lines) is still well defined and remains ± 1 . The Chern number becomes zero when $\lambda = 1 \text{ \AA}$.

As the Ge-Lu system becomes metallic at short screening lengths with highly entangled bands around the Fermi level, it is hard to figure out where the band inversion occurs exactly solely from Fig. 10. We thus introduce a parameter $0 < \eta < 1$, and make linear interpolations between the Hamiltonian at $\lambda = 5 \text{ \AA}$ with Chern number $C = \pm 1$ (denoted by H_1) and that at $\lambda = 1 \text{ \AA}$ with zero Chern number (denoted by H_0): $H(\eta) = \eta H_1 + (1 - \eta) H_0$. The energy bands around \bar{K} at different η s are shown in Fig. 11(a) and (b) for the Ge-Lu and Si-La systems respectively. In particular, for the Ge-Lu system the gap at \bar{K} is closed at $\eta_c = 0.08$, while $\eta_c = 0.045$ for the Si-La system. The gap closure at each \bar{K} leads to a transfer of Chern number of ± 1 . By virtue of the spontaneous C_3 symmetry breaking (as discussed in Sec. III), the Chern-number transfer at two of the three \bar{K} points

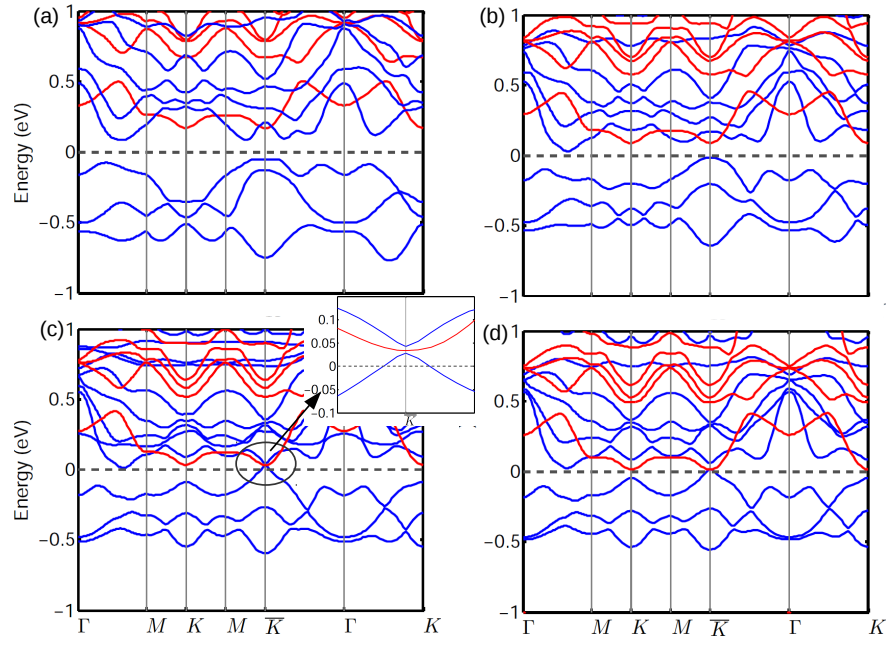


FIG. 9: The bandstructures without SOC for the Si-La system at different screening lengths λ : (a) $\lambda = 2.5 \text{ \AA}$, (b) $\lambda = 1.67 \text{ \AA}$, (c) $\lambda = 1.25 \text{ \AA}$, and (d) $\lambda = 1 \text{ \AA}$. The blue and red lines represent the spin-majority and spin-minority bands.

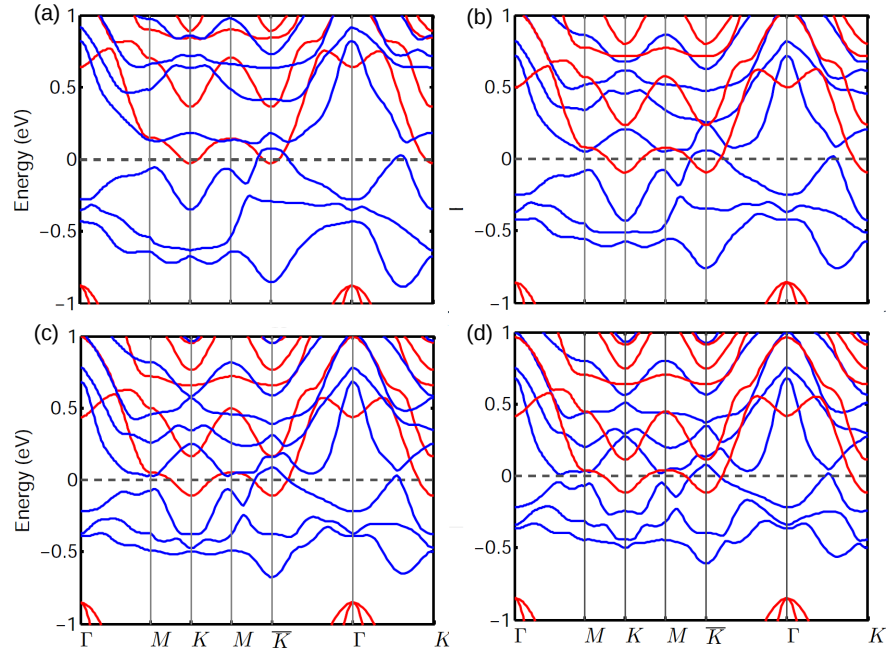


FIG. 10: The bandstructures without SOC for the Ge-Lu system at different screening lengths λ : (a) $\lambda = 2.5 \text{ \AA}$, (b) $\lambda = 1.67 \text{ \AA}$, (c) $\lambda = 1.25 \text{ \AA}$, and (d) $\lambda = 1 \text{ \AA}$. The blue and red lines represent the spin-majority and spin-minority bands.

are the same, and are opposite to that at the third \bar{K} point. Thus the resulted topological phase has

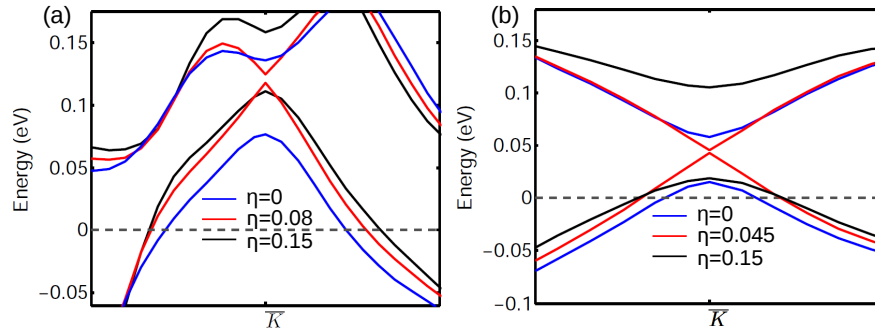


FIG. 11: The spin-majority bandstructures without SOC of the linearly interpolated Hamiltonians $H(\eta)$ between $\lambda=1 \text{ \AA} (\eta=0)$ and $\lambda=5 \text{ \AA} (\eta=1)$: (a) for the Ge-Lu system , and (b) for the Si-La system.

a Chern number of ± 1 .

-
- [1] V. Carteaux, F. Moussa, and M. Spiesser, *EPL (Europhysics Letters)* **29**, 251 (1995).
 - [2] V. Carteaux, D. Brunet, G. Ouvrard, and G. Andre, *Journal of Physics: Condensed Matter* **7**, 69 (1995).
 - [3] L. Casto, A. Clune, M. Yokosuk, J. Musfeldt, T. Williams, H. Zhuang, M.-W. Lin, K. Xiao, R. Hennig, B. Sales, et al., *APL Materials* **3**, 041515 (2015).
 - [4] J. Heyd, J. E. Peralta, G. E. Scuseria, and R. L. Martin, *The Journal of chemical physics* **123**, 174101 (2005).
 - [5] C. Franchini, R. Podloucky, J. Paier, M. Marsman, and G. Kresse, *Phys. Rev. B* **75**, 195128 (2007).
 - [6] A. A. Mostofi, J. R. Yates, Y. S. Lee, I. Souza, D. Vanderbilt, and N. Marzari, *Computer Phys. Comm.* **178**, 685 (2008).
 - [7] N. Marzari, A. A. Mostofi, J. R. Yates, I. Souza, and D. Vanderbilt, *Rev. Mod. Phys.* **84**, 1419 (2012).
 - [8] M. L. Sancho, J. L. Sancho, J. L. Sancho, and J. Rubio, *Journal of Physics F: Metal Physics* **15**, 851 (1985).
 - [9] X. Wang, J. R. Yates, I. Souza, and D. Vanderbilt, *Phys. Rev. B* **74**, 195118 (2006).
 - [10] J. P. Perdew, K. Burke, and M. Ernzerhof, *Phys. Rev. Lett.* **77**, 3865 (1996).
 - [11] A. I. Liechtenstein, V. I. Anisimov, and J. Zaanen, *Phys. Rev. B* **52**, R5467 (1995).
 - [12] J. Heyd, G. E. Scuseria, and M. Ernzerhof, *The Journal of Chemical Physics* **118**, 8207 (2003).
 - [13] P. Fazekas, *Lecture Notes in Physics* **5**, 650 (1999).
 - [14] J. Kanamori, *Progress of Theoretical Physics* **30**, 275 (1963).
 - [15] A. Ruegg and G. A. Fiete, *Phys. Rev. B* **84**, 201103 (2011).
 - [16] R. M. Martin, *Electronic structure: basic theory and practical methods* (Cambridge university press, 2004).
 - [17] Again, the Wannier functions of the tight-binding models are obtained by projecting the Bloch functions onto atomic orbitals (then Fourier transform), so that the Wannier functions can be considered as atomic orbitals localized at the atomic sites.